Electronic structure of the N donor center in $4H$-SiC and $6H$-SiC

A. v. Duijn-Arnold, R. Zondervan, and J. Schmidt

*Centre for the Study of the Excited States of Molecules, Leiden University, Huygens Laboratory,
P.O. Box 9504, 2300 RA Leiden, The Netherlands*

P. G. Baranov and E. N. Mokhov

A.F. Ioffe Physico-Technical Institute, St. Petersburg, Russia

In this paper, we present high-frequency (95 GHz) pulsed electron paramagnetic resonance (EPR) and electron nuclear double resonance (ENDOR) measurements on the nitrogen (N) donor in $4H$-SiC (k site) and $6H$-SiC (h, k_1, and k_2 sites according to the accepted classification). From the isotropic (a) and anisotropic (b) hyperfine interaction of the unpaired electron spin of the donor with the ^{13}C (35% ^{13}C-enriched samples were used) and ^{29}Si nuclei, the distribution of the electronic wave function of the N donor is determined. It is found that this wave function is quite different in the two polytypes because the spin-density distribution over the ^{13}C and ^{29}Si nuclei differs between the $4H$ and $6H$ polytypes. A similar conclusion was derived from the EPR line broadening of the N donor in ^{13}C-enriched $4H$- and $6H$-SiC compared with nonenriched crystals. The main part of the spin density in $4H$-SiC is located on the Si sublattice and the wave function contains a relatively large portion of Si p character. A tentative assignment is proposed for five ENDOR lines. For the three sites in $6H$-SiC, the main part of the spin density is located on the C sublattice and the wave function is built mostly of s-like C atomic orbitals. Comparing the three sites in $6H$-SiC, the h site wave function has the largest delocalization and is most isotropic. The k_2 site wave function is most localized and less isotropic. The largest part of the spin density is located far into the crystal. The difference in behavior of the wave function in $4H$ and $6H$ polytypes seems to find its origin in the difference in their conduction-band structure. Our results indicate that the conduction-band minima in $4H$-SiC (bottom of the conduction bands) are mainly Si-like, whereas in $6H$-SiC the conduction-band minima are mostly C-like.

I. INTRODUCTION

Silicon carbide (SiC) is a promising wide-band-gap semiconductor for applications in high-frequency, high-temperature, and high-power electronic devices. For this purpose, n- and p-type SiC is grown by incorporation of donor impurities, like N, or acceptor impurities, like B, Al, and Ga. To further the development of such semiconducting devices, a good understanding of the electronic and geometric properties of the created donor and acceptor centers is imperative. A complicating factor in such studies is that SiC can occur in different polytypes, with greatly different band structures, and also that the donor and acceptor impurities seem to occur at different sites in the polytypes.

An important issue is the spatial delocalization of the electronic wave function of the donor and acceptor centers in semiconductors. The method of choice to obtain this information is electron nuclear double resonance (ENDOR) spectroscopy developed by Feher,[1] which has been applied to donor impurities in Si by Feher,[1] Fletcher *et al.*,[2] Hale, Ivey, and Mieher,[3] and to acceptor impurities in SiC by Duijn-Arnold *et al.*[4] In these experiments, the hyperfine (hf) interaction between the unpaired electron spin of the donor and the nuclear spin of the surrounding atoms is determined, which is then translated into the spin density of the electronic wave function at the various atomic positions.

In this paper, we present the results of an ENDOR study of the N-donor center in $4H$-SiC and $6H$-SiC. The N donor in SiC has been studied extensively using optical absorption and emission spectroscopy by Choyke, Hamilton, and Patrick[5] and using Raman experiments by Colwell and Klein.[6] The first electron paramagnetic resonance (EPR) measurements on the N donor in SiC were done by Woodbury and Ludwig[7] and the first ENDOR measurements were done by Hardeman and Gerritsen[8,9] both at 9.5 GHz. High-frequency EPR measurements at 142 GHz by Kalabukhova, Kabdin, and Lukin[10] allowed to separate overlapping EPR lines, owing to the high spectral resolution, and to assign the various EPR lines to specific sites in SiC lattice. Additional ENDOR measurements were reported by Greulich-Weber *et al.*[11] An overview of our current knowledge of the electronic properties of the N-donor, obtained by EPR and ENDOR at 9.5 GHz, is found in the review papers by Greulich-Weber.[12]

The important aspect of the ENDOR investigation presented here is that it has been performed at a microwave frequency of 95 GHz, i.e., ten times higher than the conventional frequency of 9.5 GHz at which all ENDOR measurements reported so far have been carried out. The great advantage of this high microwave frequency is that the high spectral resolution not only allows us to distinguish the various sites in the EPR spectra, but it also leads to a separation of the ENDOR signal of the ^{13}C ($I=\frac{1}{2}$) and ^{29}Si ($I=\frac{1}{2}$) nuclei. Thus the hf interaction of the unpaired electron spin with the surrounding nuclear spins can be determined in great detail supplying information from which the spatial delocalization of the electronic wave function can be obtained.

The interpretation of the ENDOR data on the N donor in SiC presents a considerable problem because the assignment of the ENDOR lines to specific nuclei is complicated. This is related to the fact that the N-donor electronic wave function is a linear combination of the wave functions in the six minima of the conduction band. As a result, interference effects occur, which means that the overall density of the wave function does not decay monotonically with the distance to the N donor. As yet we have not been able to come to an unambiguous assignment of the observed ENDOR lines to specific nuclei. Nevertheless, by comparing the general aspects of the ENDOR spectra with theoretical predictions of the electronic spin-density distribution based on the Kohn-Luttinger theory[13,14] for describing donor states, we are able to present tentative explanations for the differences in the behavior of the N donor at the k site in $4H$-SiC and the h, k_1, and k_2 sites in $6H$-SiC. Moreover, for the k-site N donor in $4H$-SiC we present an assignment of the first five ENDOR lines to shells, using the similarity of this site with the P (As,Sb) donors in Si as investigated by Feher.[1]

II. EXPERIMENT

The electron paramagnetic resonance (EPR) and electron nuclear double resonance (ENDOR) measurements were performed on five different $4H$-SiC and five different $6H$-SiC samples, doped with N and with ^{13}C in natural abundance and enriched to $\sim35\%$. In view of the overwhelming amount of work the orientational dependence of the ENDOR lines was only studied in the ^{13}C-enriched sample exhibiting the strongest ENDOR signal intensity. Due to their relaxation characteristics, the nonenriched samples were not suitable for pulsed ENDOR experiments.

The samples were free-standing epitaxial layers grown by the sublimation sandwich method[15] in vacuum at temperatures between 1700 and 1750 °C. The two polytypes were grown under the same conditions and in each the N concentration was 10^{17} cm^{-3}.[16] At this low concentration, no N pairs are created. To ensure that no other polytypes are mixed in, the visible photoluminescence (PL) was monitored using optical microscopy. With this method, polytype inclusions as small as 1 μm can be detected. Also PL experiments of vanadium proved that no other polytypes were mixed in. Further proof that the samples consisted of one polytype is provided by the observation of the characteristic hf patterns in the N-donor EPR spectra (see the following section, Fig. 2). The high ^{13}C enrichment was accomplished using polycrystalline SiC with ^{13}C enriched to about 50% as source material, which was placed close (~0.5 mm) to the substrate during growth.[15] The $4H$-SiC sample also contained a small concentration of boron as a trace impurity, which allowed for an accurate determination of the ^{13}C enrichment from the ^{13}C hf lines in the EPR spectrum.[17] In $6H$-SiC, the enrichment was determined using the same method.

The experiments were performed at 1.2 K on a home-built, pulsed EPR/ENDOR spectrometer operating at a microwave frequency of 95 GHz.[18] The main advantages of this spectrometer are the high resolution in both the EPR and the ENDOR measurements and, owing to the split-coil configu-

ration of the superconducting magnet, the possibility to perform a complete orientational study in the mutually perpendicular planes. The orientational study was facilitated by the possibility to mount the crystal with a high precision owing to the fact that the crystal was cut perpendicular to the c axis and to the fact that the cleaved edge of the sample allowed for a precise rotation in the $(1\ 1\ \bar{2}\ 0)$ plane. The pulsed electron-spin-echo (ESE) -detected EPR spectra were measured using a two-pulse echo experiment, in which the electron spin-echo intensity is monitored as a function of the magnetic field. In the pulsed ENDOR experiment, a Mims-type pulse sequence was used. It consists of three $\pi/2$ microwave pulses with separation τ and T between the first and the second and the second and the third pulse, respectively,[19] and creates a stimulated echo (SE) at a time τ after the last pulse. Typical values for τ and T are 70 ns and 500 μs, respectively. A radiofrequency (rf) pulse, which is applied between the second and the third microwave pulse, induces a change in the intensity of the SE when this rf pulse is resonant with a nuclear transition. The ENDOR spectra are obtained by monitoring the SE intensity as a function of the frequency of the rf field.

III. RESULTS AND ANALYSIS

A. EPR spectra

SiC exists in different polytypes, resulting from a difference in the stacking sequence of the Si and C layers that build up the crystal. In $4H$-SiC, the difference in the stacking sequence leads to the formation of two nonequivalent crystallographic positions, one hexagonal (h) and one quasicubic (qc) site. In $6H$-SiC, three nonequivalent positions are formed, one hexagonal and two qc ones, called h, k_1, and k_2. We succeeded to investigate N donors in the k site (N$_k$) in $4H$-SiC and in the h, k_1, and k_2 sites (N$_h$, N$_{k1}$, and N$_{k2}$) in $6H$-SiC (the EPR signal for the h site in $4H$-SiC was too weak for ENDOR investigations).

Figure 1 shows the EPR spectra of the N donor in nonenriched and ^{13}C-enriched $4H$-SiC (a) and $6H$-SiC (b) as measured at 1.2 K and 95 GHz for two different extreme orientations of the magnetic field in the crystal. In the upper panels, the magnetic field is parallel to the c axis ($\mathbf{B}\|\mathbf{c}$). In the lower panels, the magnetic field lies in the plane perpendicular to the c axis ($\mathbf{B}\perp\mathbf{c}$). In the $4H$-SiC crystal, it is possible to determine the exact orientation in this plane using the anisotropy of the weak EPR signal of the shallow B acceptor. This EPR signal does not produce measurable ENDOR signals. For this crystal, the magnetic field in Fig. 1(a) is oriented parallel to the projection of one of the N-Si bonds in the plane perpendicular to the c axis. In both crystals, the N g tensor is axially symmetric and its principal axis lies parallel to the c axis. Due to the hf interaction of the unpaired electron spin with the N-donor nucleus, the EPR lines are split into three lines. The central hf lines of the different EPR signals are marked using the following abbreviations: N$_k$ for the N donor with N substituting on a quasicubic site in the $4H$-SiC crystal, and N$_{k1}$ and N$_{k2}$ for the N
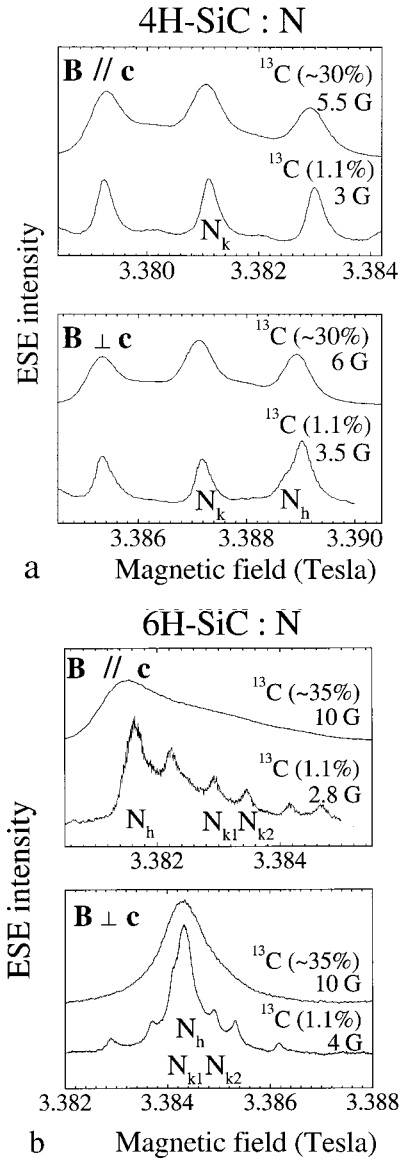
FIG. 1. The EPR spectra of the N donor in nonenriched and ^{13}C-enriched $4H$-SiC (a) and $6H$-SiC (b) as measured at 1.2 K and 95 GHz for **B∥c** (upper panels) and **B⊥c** (lower panels). In each panel, the upper spectrum is connected to the ^{13}C-enriched sample and the lower one to the nonenriched sample. The linewidth as well as the enrichment are indicated for every spectrum. The central hf EPR line (of the hf triplet) connected to the qc sites is indicated by N_k ($4H$-SiC) or N_{k1} or N_{k2} ($6H$-SiC), respectively. The hf splitting of the h-site EPR line is too small to be resolved in EPR. The one line connected to the h site is indicated by N_h but is hardly visible in the spectrum.

donor with N substituting on the qc k_1 or k_2 site in $6H$-SiC crystal, respectively. N_h indicates the signal related to a N substituting on a hexagonal site in the $4H$-SiC or $6H$-SiC crystal. For the h sites, the splitting is so small that it is not resolved in the EPR spectra. For N_k in $4H$-SiC, the splitting is 19 G, and for N_{k1} and N_{k2} in $6H$-SiC the splitting is roughly 12.3 and 12.5 G, respectively. The experimental g and hf interaction values for the N donor are in agreement with the values found in the literature.

From Figs. 1(a) and 1(b), it is clear that the spectral changes due to the ^{13}C enrichment are very different in the two polytypes. In $4H$-SiC, a slight broadening of the EPR line is observed. In $6H$-SiC, however, the linewidth is increased more than three times in the spectrum for **B∥c**. In EPR measurements at 9.5 GHz, a similar increase in linewidth is observed from 1.4 G in nonenriched $6H$-SiC to 5.5 G in ^{13}C-enriched $6H$-SiC. From the EPR results, we conclude that in $4H$-SiC the main part of the spin density resides on Si atoms because the 35% ^{13}C enrichment leads to a small line broadening. In contrast, in $6H$-SiC we conclude that the main part of the spin density of the N donor is located on the C atoms, because of the large line broadening upon 35% ^{13}C enrichment. In the latter sample, the linewidth of the nonenriched sample is slightly less than in $4H$-SiC, suggesting that there is less spin density on the Si atoms. In the discussion section, we will show that with the available ^{13}C and ^{29}Si ENDOR data a reasonable value for the observed linewidth is found.

B. ENDOR spectra

The EPR and ENDOR data for the N donors in SiC can be described by a spin Hamiltonian of the following form:

$$H = \mu_B \mathbf{S} \cdot \overleftrightarrow{g} \cdot \mathbf{B} + (\mathbf{S} \cdot \overleftrightarrow{A}_N - \gamma_N \mathbf{B}) \cdot \mathbf{I}_N + \mathbf{I}_N \cdot \overleftrightarrow{P}_N \cdot \mathbf{I}_N$$

$$+ \sum_K (\mathbf{S} \cdot \overleftrightarrow{A}_K - \gamma_K \mathbf{B}) \cdot \mathbf{I}_K,$$

where $\overleftrightarrow{A}_N$ represents the hyperfine tensors of the ^{14}N ($I=1$), $\overleftrightarrow{A}_K$ represents the hyperfine tensors of the ^{13}C ($I=\frac{1}{2}$) nuclear spins, $\overleftrightarrow{P}_N$ is the quadrupole tensor of the ^{14}N spins, γ_N is the magnetogyric ratio for the N nucleus, and γ_K is the magnetogyric ratio for the C and Si nuclei. Assuming that the hyperfine tensors have nearly axial symmetry, we can write for the hyperfine tensor $A_{zz} = a + 2b$, $A_{yy} = a - b - b'$, and $A_{xx} = a - b + b'$.[20] For the quadrupole interaction term, we can write in the principal axis system, assuming axial symmetry, P_N ($I_z^2 - \frac{1}{3} I^2$) with $P_N = \frac{3}{2} P_{zz} = 3q$ and $p_{xx} = P_{yy} = -q$. The deviation from axial symmetry is described by $q' = \frac{1}{2}(P_{xx} - P_{yy})$, $P_{xx} = -q + q'$, and $P_{yy} = -q - q'$.

The angle θ is defined as the angle between the magnetic field and the c axis; ϕ is the angle in the plane perpendicular to the c axis. The laboratory axis system is oriented as follows (see also Fig. 9). The z axis is parallel to the c axis, and $\theta = 0°$ and $\phi = 0°$. The x axis lies in the $(1\,1\,\bar{2}\,0)$ plane, parallel to the projection of a B-main C^4 bond, i.e., N-Si bond, in the plane perpendicular to the c axis ($\theta = 90°$ and $\phi = 0°$). The y axis stands perpendicular to the x axis in the plane perpendicular to the c axis ($\theta = 90°$ and $\phi = 90°$).

In Fig. 2, the complete ENDOR spectrum is presented as measured on the central hf EPR line of the N_k donor in $4H$-Si^{13}C and of the N_n donor in $6H$-Si^{13}C for **B∥c** at 95 GHz and 1.2 K. The $4H$-SiC spectrum shows the high-frequency N_k donor hf line at $25.77 + 10.41$ MHz $[=A/2 + \nu_z(^{14}N)]$, which overlaps with the ^{13}C nuclear Zeeman frequency. In the $6H$-SiC spectrum, the two high-frequency N_{k1} and N_{k2} donor hf interaction lines are indicated by ar-
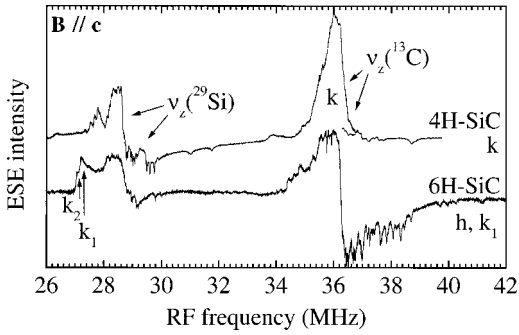
FIG. 2. The ENDOR spectra measured on the N_k donor (central hf EPR line) in $4H$-Si^{13}C and on the N_h donor (position 2, see text) in $6H$-Si^{13}C for **B**∥**c** at 95 GHz and 1.2 K. The high-frequency N_k donor hf line is located at $25.77 + 10.41$ MHz $[=A/2 + \nu_z(^{14}N)]$ (and overlaps with the ^{13}C nuclear Zeeman frequency), the high-frequency N_{k1} and N_{k2} donor hf lines are indicated by arrows. Symmetrically around the ^{29}Si and ^{13}C Zeeman frequency, ENDOR lines are seen which are due to the hf interaction of the unpaired electron spin with the ^{29}Si and ^{13}C nuclear spins in the surrounding of the N nucleus, respectively.

rows. The ^{29}Si nuclear Zeeman frequency, ν_{Si}, and the ^{13}C nuclear Zeeman frequency, ν_C, are also indicated. Symmetrically around the ^{29}Si and ^{13}C Zeeman frequency, lines are seen that are due to the hf interaction of the unpaired electron spin with the ^{29}Si and ^{13}C nuclear spins, respectively, in the surrounding of the N nucleus. In the $4H$-SiC sample, all ENDOR spectra were measured on the central N-donor hf EPR line as they are similar to those obtained on the outer two hf lines and because they are most intense. In $6H$-SiC, measurements were performed at two positions for **B**∥**c**: at 3.3815 T, i.e., on the hf EPR line of N_h, which overlaps partly with the low-field N_{k1} hf line (defined as position 2), or at 3.3822 T, i.e., the low-field hf EPR line of N_{k2}, which overlaps with the left and central k_1-site hf EPR line and partly with the h-site line (defined as position 1). At position 2, there might also be a weak overlap with the flank of the low-field hf line of N_{k2}. Comparing the spectra, we see that the signal-to-noise ratio of the ^{29}Si ENDOR lines in $4H$-SiC is much better than that in $6H$-SiC. This is remarkable because the ^{29}Si abundance (4.7%) and the EPR line strength are the same in both samples. In contrast, the ^{13}C ENDOR lines are much stronger in the $6H$-SiC sample than in the $4H$-SiC sample.

Figure 3(a) shows the comparison between the ^{13}C ENDOR spectrum with **B**∥**c** for the different sites in $4H$-Si^{13}C and $6H$-Si^{13}C. Only the spectrum on the high-frequency side of the ^{13}C Zeeman frequency is shown. The upper spectrum k belongs to the N_k donor in $4H$-SiC. The positions of the lines have been marked by diamonds. The middle spectrum, indicated by (1), was measured at position 1 in $6H$-SiC. The lower spectrum was measured at position 2 (2) (see above). By comparing the relative intensities of the ENDOR lines in the last two spectra, it is possible to make an assignment of ENDOR lines to the different sites in $6H$-SiC. When going from the lower spectrum to the middle one, the h-site-related ENDOR lines get much weaker, the k_1-site-related lines get slightly weaker, and the
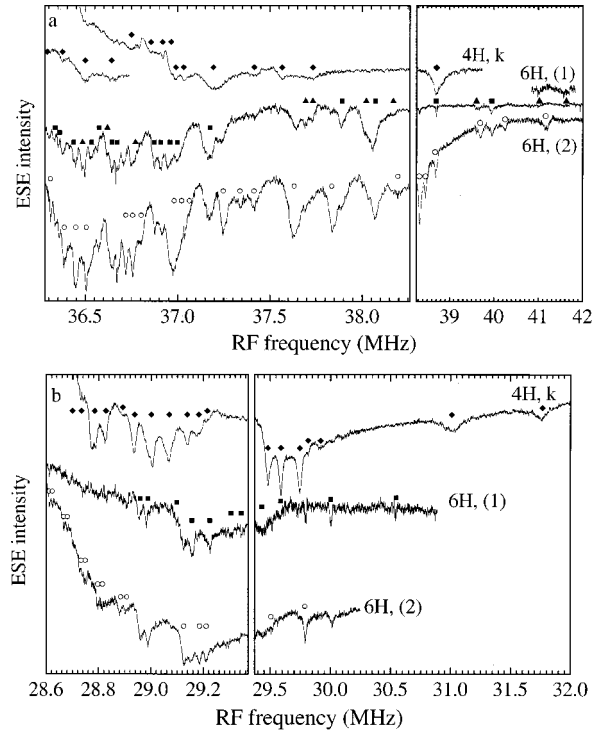

FIG. 3. The ENDOR spectra of the sites in $4H$-Si^{13}C and $6H$-Si^{13}C for **B**∥**c** at 1.2 K and 95 GHz. (a) shows the ^{13}C ENDOR lines and (b) shows the ^{29}Si ENDOR lines. In both parts, only the high-frequency side of the Zeeman frequency is shown. The upper spectrum belongs to the N_k donor in $4H$-SiC. The middle spectrum is measured at position 1 (1, see text), the lower one at position 2 (2, see text). In (a), the positions of the lines of the k site have been marked by diamonds, those of the h site by open circles, those of the k_1-site lines by filled squares, and those of the k_2 site by filled triangles. In (b), no distinction can be made between the two qc sites, due to the low signal-to-noise ratio. The k_1/k_2-site lines are both marked by filled squares.

k_2-site-related lines appear or become stronger. The positions of the h-site lines are marked by open circles, those of the k_1-site lines by filled squares, and those of the k_2 site by filled triangles.

Figure 3(b) shows the comparison between the ^{29}Si ENDOR spectrum with **B**∥**c** for the different sites in $4H$-Si^{13}C and $6H$-Si^{13}C. Only one side of the Zeeman frequency is shown. As in Fig. 3(a), the upper spectrum belongs to the N_k donor in $4H$-Si^{13}C. The lines have been marked by diamonds. The middle spectrum was measured at position 1 and the lower one at position 2 (see above). Again, an assignment to the different sites in $6H$-SiC might be attempted by comparing the last two spectra. However, due to the low signal-to-noise ratio, this is very difficult. The figure does show a distinction between h-site lines (open circles) and k_1/k_2-site lines (filled squares) but, in contrast to the preceding figure, the two qc sites could not be assigned more specifically.

From Figs. 3(a) and 3(b), it is clear that the spin-density distribution of the N-donor electron over the ^{13}C and ^{29}Si nuclei differs between $4H$-SiC and $6H$-SiC (as expected from the EPR spectra). Whereas the main part of the spin

TABLE I. The experimental values of the ionization energy of the N donors, the g factors, the hf-tensor principal values a and b and their corresponding s and p spin densities, and the quadrupole parameters q in $3C$-SiC, $4H$-SiC, and $6H$-SiC from the review by Greulich-Weber[12] and this work (indicated by $*$). For comparison, the same parameters are presented for the P and As shallow donors in silicon after Feher.[1]

SiC polytype	Site	Ionization energy E_g (meV)	$g_\parallel$	$g_\perp$	a (MHz)	b (MHz)	q (MHz)	s (%)	p (%)
$3C$-SiC	k	54	2.0050	2.0050	3.5			0.19	
$4H$-SiC	h	52.1	2.0055	2.0043	2.9	0.080		0.16	0.14
	k	91.8	2.0010	2.0013	50.97	0.004	~ 0	2.8	0.007
$6H$-SiC	h	81	2.0048	2.0028	2.47	0.137	0.017	0.14	0.25
					2.52*	0.12*	0.019*	0.14	0.22
	k_1	137.6	2.0040	2.0026	33.221	0.004	0.007	1.83	0.007
	k_2	142.4	2.0037	2.0030	33.564	0.009	0.007	1.85	0.016
silicon									
P		44	1.99850		117.53			0.9	
As		49	1.99837		198.35			1.35	

density is localized on the ^{29}Si atoms for the k site in $4H$-SiC (as expected for a donor electron), it is localized mainly on the ^{13}C atoms in the case of the $6H$-SiC sites. Note also that the spectrum of $6H$-SiC contains more lines around the ^{13}C Zeeman frequency (even though this spectrum shows the lines of three sites) than the spectrum of $4H$-SiC does around either the ^{13}C or ^{29}Si Zeeman frequency.

^{14}N *ENDOR*

The results of the EPR and ENDOR investigations of the isotropic (a) and anisotropic (b) hf and quadrupole (q) interactions with the ^{14}N nucleus for the N donors in the main SiC polytypes $3C$, $4H$, and $6H$ are presented in Table I. The values are taken from the review of Greulich-Weber[12] and from this study. Only for the h site in $6H$-SiC do we observe a small difference in the parameters (Table I). Table I also shows the experimental values of the ionization energy of the N donors, the g factors, and the s and p spin densities corresponding to the a and b hf interaction parameters of the unpaired electron with the ^{14}N nuclei in $3C$-, $4H$-, and $6H$-SiC. For comparison, the same parameters are presented for the P and As shallow donors in Si after Feher.[1] There the g factor and hf interaction are isotropic. From Table I, one can see that in general the value of the ionization energy for different sites does not correlate with the hf interactions, i.e., with the spin densities on the N nuclei. For instance, the ionization energies for the k site in $4H$-SiC and the h site in $6H$-SiC are approximately equal, but the N hf interaction for the k site in $4H$-SiC is about 20 times larger than that for the h site in $6H$-SiC.

$4H$-SiC: ^{29}Si *ENDOR*

In Fig. 4, the ^{29}Si ENDOR orientational dependence is presented of the k site in $4H$-SiC in the $(1\ 1\ \bar{2}\ 0)$ $(=zx)$ plane. For the spectra, θ is indicated on the right. The ^{29}Si ENDOR orientational dependence was also measured in the

$(0\ 0\ 0\ 1)$ plane for all lines. In Fig. 4, as well as in all the figures that follow, the spectra have been corrected for the shift of the nuclear Zeeman frequency with respect to the orientation **B**∥**c**. This shift is due to the change in the magnetic-field position of the EPR line for different orientations, which is connected to the anisotropy of the g tensor. As can be seen, the dependence of the outermost line is difficult to follow when we turn away from the c axis due to the low signal-to-noise ratio. To enable a fit of the dependence, this line was also measured in the $(\bar{1}\ 1\ 0\ 0)$ $(=zy)$ plane, which is perpendicular to the two previous planes. For all other lines, the dependence was clear enough using only the dependences in the $(1\ 1\ \bar{2}\ 0)$ and $(0\ 0\ 0\ 1)$ planes. Due to a lack of space, not all measured orientations are shown in Fig. 4.

Figures 5(a)–5(c) show the experimental data points, corrected for the nuclear Zeeman shift, for all measured orientations and the fits to these points as made using the program "Visual EPR 12.08 professional edition" written by
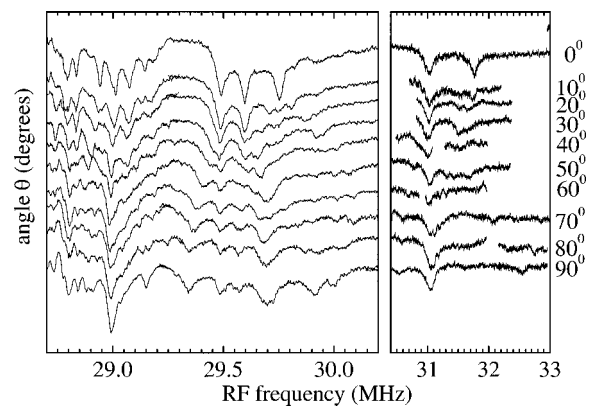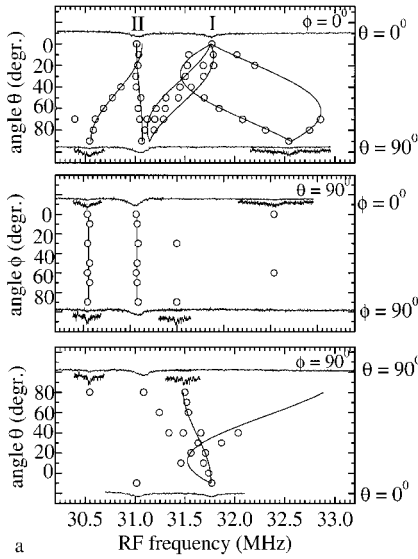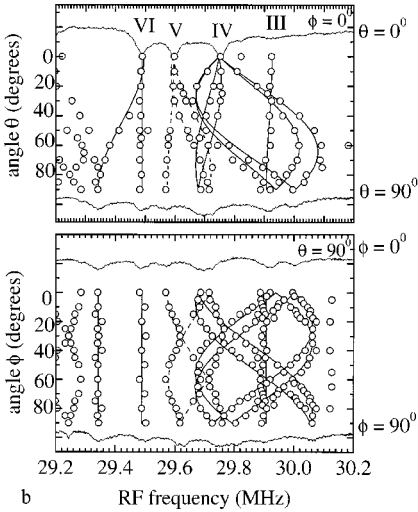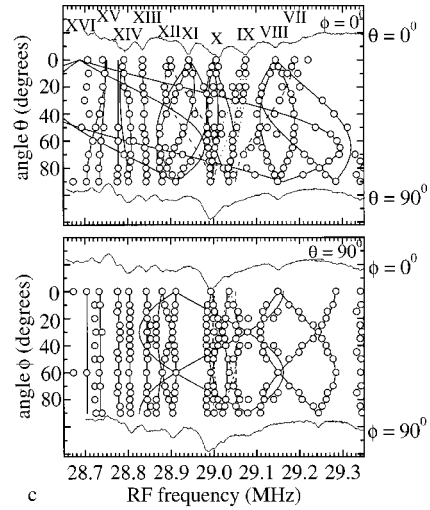

FIG. 4. The orientational dependence of the ^{29}Si ENDOR lines of the k site in $4H$-SiC in the $(1\ 1\ \bar{2}\ 0)$ $(=zx)$ plane. For the spectra, θ is indicated on the right. The spectra have been corrected for the shift of the nuclear Zeeman frequency with respect to the orientation **B**∥**c**. Not all measured orientations are shown.

FIG. 5. The experimental data points of the orientational dependence of the ^{29}Si ENDOR lines, corrected for the nuclear Zeeman shift, for all measured orientations and the fits to these points for the k site in $4H$-SiC. In total, 16 patterns have been found. They belong to 16 different groups of nuclei and are numbered using roman numbers. On the right, θ and ϕ are indicated for the spectra. For the experimental data points, the angle is indicated on the left side. The fixed angle is indicated in the panels. (a) shows the orientational dependence of groups I and II in the zx and zy and zx and xy plane, respectively, (b) shows the dependence of groups III–VI in the zx and xy plane, and (c) shows that of groups VII–XVI in the zx and xy plane. In places where the fits of different lines overlap, dotted or dashed lines have been used instead of full ones to clarify the dependences. Table II contains for every group the roman number, the hf-tensor principal values, and the Euler angles of the hf tensor.

4H-SiC: ^{13}C *ENDOR*

Figure 6 shows the orientational dependence of the ^{13}C ENDOR lines connected to the k site in $4H$-Si^{13}C as measured at 95 GHz and 1.2 K. The figure shows the spectra along the three main axes in the crystal: the c axis, the x, and the y axis. The points give the positions of the lines and are corrected for the shift of the nuclear Zeeman frequency with θ. In contrast to the ^{29}Si ENDOR orientational dependence, only five ^{13}C hf lines show a frequency shift in the $(1\,1\,\bar{2}\,0)$ plane. All lines are isotropic in the $(0\,0\,0\,1)$ plane. Only for the orientationally dependent lines, points are shown at all measured orientations. To clearly show lines XII–XIV, the spectrum on the right side of the Zeeman frequency is shown a second time with the N-donor hf ENDOR line subtracted. The 14 groups found in this dependence are numbered with roman numbers. Due to a lack of space in the figure, the numbers VI–XII are not put next to the lines. The hf fit values of groups I–XIV can be found in Table III.

6H-SiC: ^{13}C *ENDOR*

Figure 7 shows the ^{13}C orientational dependence of the three sites h, k_1, and k_2 in $6H$-Si^{13}C as measured at 95 GHz

Grachev.[21] In places where the fits of different lines overlap, dotted or dashed lines are used instead of full ones to clarify the dependences. In total, 16 patterns have been found, belonging to 16 different groups of nuclei, which are numbered using roman numbers. Table II contains for every group the roman number, the hf-tensor principal values, and the Euler angles of the hf tensor. The Euler angles are defined in the laboratory axis system in which the orientational dependences were measured. The first rotation α is around the z axis, the second one β is around the new y axis, and the third one γ is around the new z axis. Figure 5(a) shows the orientational dependences of group I (in the zx and zy plane) and group II (in the zx and xy plane). Figure 5(b) shows the dependence of groups III–VI and Fig. 5(c) that of groups VII–XVI in the zx and xy planes. On the right, θ is indicated for the experimental spectra. For the data points, θ is indicated on the left. According to crystal symmetry, the dependence in the xy plane should repeat every 60° and have "reflection" symmetry around $\varphi = 30°$. With the help of the above symmetry rules, the overlapping lines in the region around 29 MHz [Fig. 5(c)] could be disentangled. It should be noted that in the xy plane some lines are missing for group I.

TABLE II. The Euler angles, the hf-tensor principal values a and b, and the corresponding s and p spin densities of the unpaired electron connected to the k site in $4H$-SiC with the ^{29}Si nuclei surrounding the center. The numbers in the first column correspond to the numbers next to the ENDOR lines in Fig. 5. A line that cannot be described by one hf tensor (e.g., lines II, VI, XIV, and XV), because it is a superposition of two lines in the spectrum for **B**‖**c**, is numbered by a and b in the table. For comparison, the same parameters are presented for five shells of As and P shallow donors in silicon (Si) after Feher.[1]

4H-SiC, N, k	Euler angles (deg) α	β	γ	a (MHz)	b (MHz)	b' (MHz)	s (%)	p (%)
I	26, 282	70	22	6.54±0.04	1.26±0.03	0.75 ±	0.14	1.10
	154, 258	70	−22			0.02		
IIa	0	0	0	4.79±0.01	−0.041 ±		0.10	0.036
					0.008			
IIb	0	0	0	4.14±0.01	0.34±0.01		0.090	0.298
III	0	0	0	2.510 ±	0.013 ±		0.055	0.011
				0.007	0.005			
IV	23, 278, 326,	66	0	2.34±0.02	0.31±0.02		0.051	0.27
	157, 214, 262	66	0					
V	29	79	148	1.970 ±	0.122 ±	0.014 ±	0.043	0.107
	90	79	0	0.004	0.005	0.008		
	151	79	212					
VIa	0	0	0	1.66±0.02			0.036	
VIb	0	0	0	1.473 ±	0.102 ±		0.032	0.089
				0.007	0.006			
VII	0	0	0	0.88±0.02	0.09±0.01		0.019	0.079
VIII	0, 60, 120, 180	65	0	1.044 ±	0.141 ±		0.023	0.123
				0.009	0.009			
IX	0, 55, 125, 180	80	0	0.775 ±	−0.046 ±	0.020 ±	0.017	0.040
				0.007	0.005	0.007		
X	0, 60, 120, 180	60	0	0.695 ±	0.043 ±		0.015	0.038
				0.005	0.001			
XI	0, 60, 120, 180	37	0	0.502 ±	0.080 ±		0.011	0.070
				0.001	0.003			
XII	0, 180	15	0	0.614 ±	−0.077 ±	0.008 ±	0.013	0.067
				0.003	0.002	0.005		
XIII	0	0	0	0.368 ±	−0.006 ±		0.008	0.005
				0.002	0.002			
XIVa	0, 180	25	0	0.282 ±	−0.016 ±	0.004 ±	0.006	0.014
				0.003	0.003	0.003		
XIVb	0	0	0	0.242 ±			0.005	
				0.004				
XVa	0	0	0	0.165 ±	0.009 ±		0.004	0.008
				0.004	0.004			
XVb	0	0	0	0.126 ±	0.031 ±		0.003	0.027
				0.003	0.002			
XVI	0, 60, 120, 180	65	0	0.47±0.02	0.402 ±	−0.27 ±	0.010	0.35
					0.009	0.01		

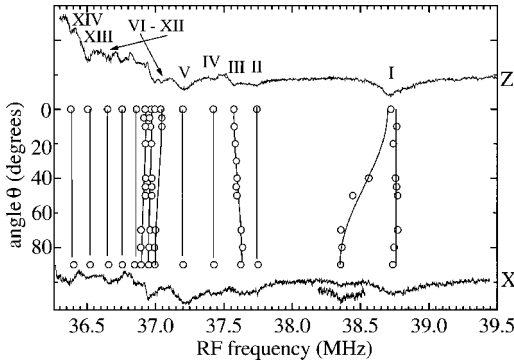| Si P, As	Shell position			a (MHz)	b (MHz)	b' (MHz)	s (%)	p (%)
P	(400)			5.96	0.034	0.028	0.13	0.03
As				7.72	0.043	0.04	0.17	0.04
P	(440)			4.52	0.056		0.10	0.05
As				6.0	0.104	−0.012	0.13	0.09
P	(333)			3.28	<0.008		0.07	<0.007
As				4.08	0.008		0.09	0.007
P	(555)			2.26	0.02		0.05	0.017
As				2.58	0.024		0.06	0.021
P	(111)							
As				1.60	1.10		0.035	0.96

FIG. 6. The orientational dependence of the ^{13}C ENDOR lines of the k site in $4H$-Si[13]C. Fourteen groups, indicated by Roman numbers, are found in this dependence. The spectra and points have been corrected for the shift of the nuclear Zeeman frequency. The spectra are shown for two main orientations, the $c(z)$ and the x axis, indicated at the right. Along the x and y axes, the spectra are identical. Only five lines showed an orientational dependence in the (1 1 $\bar{2}$ 0) plane, and all lines were isotropic in the (0 0 0 1) plane. Only for the anisotropic lines are all measured data points shown. To clearly show lines XII–XIV, the N-donor hf ENDOR line has been subtracted for that part of the spectrum. Due to a lack of space, numbers VI–XII are not indicated above the lines. The fit values are shown in Table III.

and 1.2 K. As before, all spectra and points, which represent the lines, have been corrected for the nuclear Zeeman shift. The two upper spectra in the three panels, indicated by $\theta = 0°$ on the right, show the spectra measured for **B**∥**c** at positions 1 (upper one) and 2 (lower one) in the EPR line. The middle spectrum ($\theta = 45°$) was measured on the most intense part of the EPR line. Probably the EPR lines of all sites are overlapping at this position. The lowest three spectra ($\theta = 90°$) were measured on the central part of the EPR line (see Fig. 1). The ENDOR lines of all sites are present in these spectra. Note that, in contrast to the measurements on $4H$-SiC, the exact orientation with respect to the crystallographic axis system is not known in the (0 0 0 1) plane. The lower two, indicated by $\varphi = 45°$ and $\varphi = 90°$, were measured with the magnetic field at an angle of 45° or 90°, respectively, with the magnetic-field direction of the upper spectrum. Only two nonaxial hf tensors were found, around 37.1 and 36.74 MHz. It is assumed that their hf tensor is oriented parallel to the crystallographic axis system. All other lines are found to be isotropic in the plane perpendicular to the c axis, i.e., their tensors are axially symmetric around the c axis. The open circles and full lines represent the dependences of the h site, squares and dotted lines those of the k_1 site, and triangles and dashed lines those of the k_2 site [see also Fig. 3(a)]. The fit values are presented in Table IV (h site) and Table V (k_1 and k_2 site). It should be mentioned that the exact orientation of the c axis was determined by using (one of) the orientationally dependent lines. The lines for which only three or two points are shown in the spectrum were found to be isotropic in this proces. Comparing this dependence with the [29]Si orientational dependence of the k site in $4H$-Si[13]C (Fig. 5), we see a remarkable difference. In the latter orientational dependence, most lines split when

TABLE III. The hf-tensor principal values a and b and the corresponding s and p spin densities of the unpaired electron connected to the k site in $4H$-SiC with the ^{13}C nuclei surrounding the center. The numbers in the first column correspond to the numbers next to the ENDOR lines in Fig. 6. Due to a lack of space in Fig. 6, not all lines are numbered. It is seen that, in contrast to the [29]Si hf-interaction tensors given in Table II, most tensors are isotropic. Only the orientational dependence of the anisotropic lines, I, III, VI, VIII, and IX is drawn in Fig. 6.

$4H$-SiC, N, k	a (MHz)	b (MHz)	s (%)	p (%)
Ia	5.02±0.01		0.13	
Ib	4.433±0.009	0.233±0.009	0.12	0.22
II	2.993±0.008		0.079	
III	2.724±0.005	−0.038±0.004	0.072	0.035
IV	2.370±0.005		0.063	
V	1.926±0.008		0.051	
VI	1.531±0.002	0.032±0.002	0.040	0.030
VII	1.496±0.003		0.040	
VIII	1.416±0.006	0.016±0.005	0.037	0.015
IX	1.323±0.005	0.020±0.004	0.035	0.018
X	1.215±0.006		0.032	
XI	1.015±0.004		0.027	
XII	0.826±0.007		0.022	
XIII	0.529±0.005		0.014	
XIV	0.276±0.006		0.007	

turning away from the c axis and moreover they shift over larger distances than the lines in the $6H$-SiC spectra. This suggests that, in contrast to the hf tensors of the sites in $6H$-SiC, most of the hf tensors for the k site in $4H$-SiC are not aligned with the crystallographic axis system.

6H-SiC: [29]Si *ENDOR*

Figure 8 shows the orientational dependence of the [29]Si for the three sites h, k_1, and k_2 in $6H$-Si[13]C as measured at 95 GHz and 1.2 K. Again the spectra and points have been corrected for the nuclear Zeeman shift. The upper two spectra were measured at positions 1 (upper one) and 2 (lower one) for **B**∥**c** (as indicated on the right by $\theta = 0°$), respectively. The other four spectra were measured at the angles $\angle(\mathbf{B},\mathbf{c}) = 20°$, 45°, 70°, and 90°, also indicated on the right side of the figure. The spectra were always measured on the most intense part of the EPR line. The full lines and open circles represent positions of the h-site lines and the filled squares and dotted lines those of the k_1-, or k_2-site lines. θ is indicated on the left. Due to the poor signal-to-noise ratio, no spectra could be measured in the plane perpendicular to the c axis. It is assumed that the lines are isotropic in this plane. Table IV shows the hf tensors of the ENDOR lines related to the h site. Table VI contains the hf tensors of the ENDOR
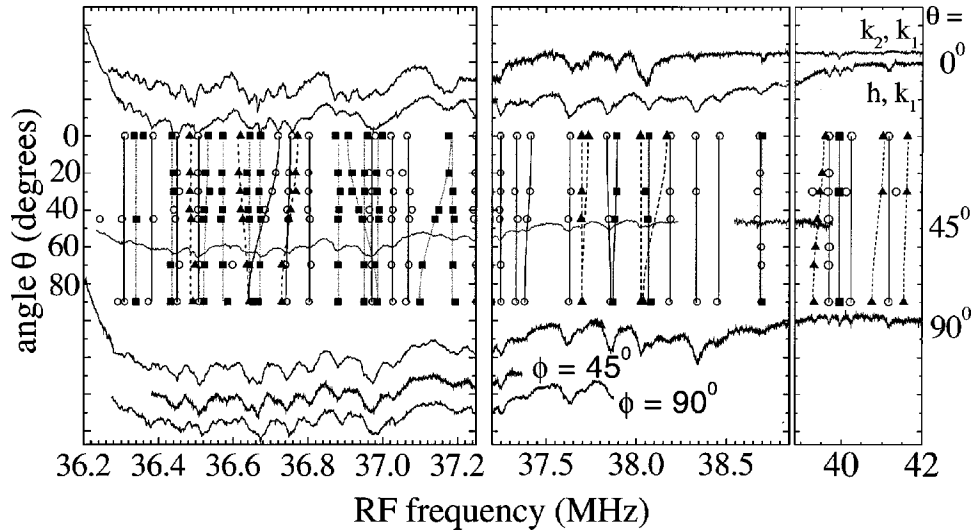
FIG. 7. The orientational dependence of the ^{13}C ENDOR lines of the three sites h, k_1, and k_2 in $6H$-Si^{13}C. The upper two, middle, and lower three spectra in the three panels are measured for $\angle(\mathbf{B},\mathbf{c})=0°$, $\angle(\mathbf{B},\mathbf{c})=45°$, and $\angle(\mathbf{B},\mathbf{c})=90°$, respectively, as indicated at the right. The upper spectrum at $0°$ is measured at position 1, the lower one at position 2. The middle spectrum $[\angle(\mathbf{B},\mathbf{c})=45°]$ is measured on the most intense part of the EPR line. The upper spectrum ($90°$) is measured on the central part of the EPR line and incorporates the lines of all sites. The lower two spectra at $90°$, indicated by $\varphi=45°$ and $\varphi=90°$, are measured with the magnetic field making an angle of $45°$ or $90°$, respectively, with the magnetic-field direction of the first spectrum in the plane perpendicular to the c axis. The ENDOR lines are represented by points, different points indicating different sites, with θ indicated on the left. All spectra and points have been corrected for the nuclear Zeeman shift. The open circles and full lines represent the dependences of the h site, squares and dotted lines those of the k_1 site, and triangles and dashed lines those of the k_2 site (see Fig. 3). The fit values are presented in Table IV (h site) and Table V (k_1 and k_2 site).

lines of the qc sites. In the figure, no distinction is made between the k_1 and k_2 site. However, in Table VI the lines that might belong to the k_2 site are marked with a star or question mark; the unmarked hf parameters belong to the k_1 site. In contrast to the $4H$-SiC ^{29}Si lines, the $6H$-SiC ^{29}Si hf lines do not seem to split; they only shift with changing orientation. It should be mentioned that the exact orientation of the c axis was determined by the orientationally dependent lines in the spectrum. The lines for which only three or two points are shown in the spectrum were found to be isotropic in this process. Only for the ^{29}Si outer ENDOR lines (Fig. 8) was it difficult to determine the orientational dependence due to the low signal-to-noise ratio.

IV. DISCUSSION

According to the EPR and ENDOR results, the electronic wave function of the N donor is found to be quite different in the two polytypes. In particular, the spin-density distribution over the ^{13}C and ^{29}Si nuclei is different for the $4H$ and $6H$ polytypes. The main part of the spin density in $4H$-SiC is located on the Si sublattice and the wave function contains a relatively large portion of Si p character. The hf tensors for many Si shells have orientations that do not coincide with the c axis and, what is more, a deviation from axial symmetry of the hf tensor has been observed for several Si shells. For each of the three sites in $6H$-SiC, the main part of the spin density is located on the C sublattice and the wave function is built mostly of s-like C atomic orbitals. The anisotropic hf tensors for the Si and C are mainly oriented parallel to the c axis, in contrast to those in $4H$-SiC. Com-

paring the three sites in $6H$-SiC, the h-site wave function has the largest delocalization. The k_2-site wave function is most localized. For the h, k_1, and k_2 sites in $6H$-SiC, the spatial distribution of the wave function of the N donors over the Si and C nuclei is qualitatively the same. In contrast, the isotropic hf interaction constant with the ^{14}N nucleus in the h site is about 15 times smaller than that for the qc sites and, at the same time, the anisotropic hf interaction constant is about 15 times larger. In $4H$-SiC, one sees the same behavior as in $6H$-SiC but the difference in the ^{14}N hf interaction between the h and k sites is even larger (a ratio of 20). We remark that, although the difference in the ^{14}N hf interaction for the h and qc sites in $4H$- and $6H$-SiC is the same, the spatial distribution of the wave function on the Si and C nuclei is very different. In passing, we note that our finding that the spin density in $6H$-SiC is located mainly on C is at variance with the conclusion of Greulich-Weber[12] that in $6H$-SiC the spin density is mainly on the Si. We explain this contradiction by the fact that at the X-band frequency (the frequency at which the ENDOR measurements were carried out) it is very difficult to assign the lines to Si or C nuclei because of the strong overlap. Moreover, since the hyperfine interaction $A/2$ is equal to the nuclear Zeeman frequency, it is very difficult or almost impossible to observe the low-frequency lines. Moreover, in our experiment we benefited from the ^{13}C enrichment.

To obtain the distribution of the electronic wave function of the N donor in the SiC crystal, the hf interactions found in the ENDOR spectra have to be assigned to specific (groups of) nuclei in the surrounding of the N donor and then trans-

TABLE IV. The hf-tensor principal values a and b and the corresponding s and p spin densities of the unpaired electron connected to the h site in $6H$-SiC with the ^{13}C and ^{29}Si nuclei surrounding the center. Comparison with Tables II and III shows that these tensors are more isotropic than the ones connected to the k site in $4H$-SiC. The tensors correspond to the full lines and open circles of Figs. 7 (^{13}C) and 8 (^{29}Si). The numbers in the first column count the lines from the line at the highest frequency (41 MHz in the ^{13}C spectrum and 29.8 MHZ in the ^{29}Si spectrum) to the line at the lowest frequency (36.4 MHZ in the ^{13}C spectrum and 27.4 MHz in the ^{29}Si spectrum). The tensor corresponding to the last line in ^{13}C is not incorporated in the table because assignment to a specific site is not possible.

$6H$-SiC N, h	^{13}C, a (MHz)	^{13}C, b (MHz)	s (%)	p (%)	^{29}Si, a (MHz)	^{29}Si, b (MHz)	s (%)	p (%)
1	9.950± 0.001		0.260		2.359± 0.007		0.051	
2	8.095± 0.002		0.21		1.821± 0.001	−0.017± 0.001	0.040	0.015
3	6.994± 0.007		0.19		1.196± 0.003		0.026	
4	4.982± 0.006		0.13		0.876± 0.004	0.124± 0.004	0.019	0.11
5	4.52± 0.01		0.12		1.019± 0.003		0.022	
6	4.275± 0.006		0.11		0.755± 0.004	−0.077± 0.004	0.016	0.067
7	3.987± 0.004		0.11		0.569± 0.002	−0.012± 0.002	0.012	0.01
8	3.309± 0.001	−0.015± 0.001	0.088	0.014	0.362± 0.005		0.008	
9	2.866± 0.008		0.076		0.248± 0.005		0.005	
10	2.392± 0.002	0.024± 0.002	0.063	0.022				
11	2.276± 0.008		0.060					
12	2.102± 0.002		0.056					
13	1.742± 0.006		0.046					
14	1.656± 0.003		0.044					
15	1.548± 0.004		0.041					
16	1.214± 0.003		0.032					
17	1.097± 0.002	0.008± 0.002	0.029	0.007				
18	0.943± 0.003	0.055± 0.004	0.025	0.051				
19	0.621± 0.002		0.016					
20	0.507± 0.008		0.013					
21	0.371± 0.004		0.010					

lated to spin densities. The assignment to specific nuclei presents a considerable problem because, as a result of the multivalley structure of the conduction band, interference effects occur, which means that the overall density of the wave function does not decay monotonically with the distance to the N donor. To describe this problem, we use a model introduced by Kohn and Luttinger.[13,14]

Before we start the discussion of the EPR and ENDOR data on the ^{13}C and ^{29}Si nuclei using the Kohn-Luttinger theory,[13,14] we will first give a qualitative analysis of the wave function as found in $4H$-SiC and $6H$-SiC on the basis of the calculated band structure[22] and the effective masses.[23–25] Figure 9 shows the reciprocal lattice of $4H$-SiC and $6H$-SiC, its symmetry points, and the orientation of this

TABLE V. The hf-tensor principal values a and b and the corresponding s and p spin densities of the unpaired electron connected to the k_1 and k_2 site in $6H$-SiC with the ^{13}C nuclei surrounding the center. Comparison with Table IV shows that the tensors are slightly more anisotropic for the qc sites than for the h site. The tensors correspond to the dashed lines and full triangles for the k_2 site and the dotted lines and full squares for the k_1 site as shown in Fig. 7. The numbers in the first column count the lines from the line at the highest frequency (41.7 MHz for k_2 and 40 MHz for k_1) to the line at the lowest frequency (36.48 MHz for k_2 and 36.34 MHz for k_1).

$6H$-SiC, N, k_2	^{13}C, a (MHz)	^{13}C, b (MHz)	^{13}C, b' (MHz)	s (%)	p (%)
1	10.75 ± 0.004	0.065 ± 0.002		0.28	0.061
2	9.318 ± 0.005	0.195 ± 0.007		0.25	0.18
3	6.383 ± 0.008	0.175 ± 0.009		0.17	0.16
4	3.771 ± 0.001	0.087 ± 0.001		0.10	0.081
5	3.659 ± 0.003			0.097	
6	3.023 ± 0.002	0.023 ± 0.002		0.080	0.021
7	3.000 ± 0.002			0.079	
8	1.066 ± 0.002	0.043 ± 0.002	0.041 ± 0.002	0.028	0.04
9	0.869 ± 0.002	-0.018 ± 0.002		0.023	0.017
10	0.579 ± 0.003			0.015	
$6H$-SiC, N, k_1					
1	7.519 ± 0.003			0.20	
2	5.009 ± 0.001			0.13	
3	3.743 ± 0.006			0.10	
4	3.366 ± 0.002	0.014 ± 0.001		0.089	0.013
5a	1.980 ± 0.005			0.053	
5b	1.820 ± 0.004	0.076 ± 0.003	0.058 ± 0.004	0.048	0.071
6	1.583 ± 0.004			0.042	
7	1.510 ± 0.003			0.040	
8	1.525 ± 0.003	-0.054 ± 0.002		0.040	0.050
9	1.369 ± 0.006			0.036	
10	0.950 ± 0.004			0.025	
11	0.892 ± 0.005			0.024	
12	0.753 ± 0.004			0.020	
13	0.656 ± 0.004	0.007 ± 0.003		0.017	0.007
14	0.480 ± 0.003			0.015	
15	0.285 ± 0.004			0.008	
16	0.222 ± 0.002			0.006	

lattice with respect to the lattice in real space. In $4H$-SiC, the minimum of the conduction band lies at the M point. The effective mass is almost axially symmetric around the direction ΓM. In the calculations, the effective masses $m_{M\Gamma} = 0.62m_0$ and $m_{MK} = m_{ML} = 0.32m_0$ (m_0 is the free-electron mass) were used. The position of the minimum in $6H$-SiC is less clear but it is agreed that it should be between the M and L point. Thus the conduction band of $6H$-SiC has minima in the six possible $(1\,1\,\bar{2}\,0)$ planes of the crystal, and in the calculations it is assumed that the minima lie at 60% from M to L. In $6H$-SiC, the effective mass is not axial: $m_{M\Gamma} = 0.77m_0$, $m_{MK} = 0.24m_0$, and $m_{ML} = 1.7m_0$. An average in-plane mass $m_\perp$ (perpendicular to the c axis) which is built up from the longitudinal mass m_1 (along the Γ-M direction) and the transverse mass m_t (along the M-K direction) is given by $m_\perp = \sqrt{m_{M\Gamma} m_{MK}}$.[26] In $4H$-SiC, $m_\perp = 0.445m_0$ and in $6H$-SiC, $m_\perp = 0.43m_0$. Thus one can see that the planar

masses are almost the same for the $4H$ and $6H$ polytypes, though there exists a considerable difference in the effective masses along the c axis. In $4H$-SiC, the effective mass along the c axis is $m_{ML} = 0.32m_0$, which is close to the planar mass, but in $6H$-SiC the effective mass along the c axis is $m_{ML} = 1.7m_0$. These properties of the effective masses explain why for $4H$-SiC the wave function of shallow donors should be roughly spherically symmetric, whereas for $6H$-SiC it should be strongly compressed along the c axis. Moreover, the "effective" Bohr radius of the wave function is given by $a^* = [\kappa/(m^*/m_0)]a_0$, where $a_0 = 0.5292$ Å (the Bohr radius), and its ionization energy is given by $E_{\text{eff}} = [(m^*/m_0)/\kappa^2]E_0$, with E_0 the Rydberg energy. In $4H$-SiC, $\kappa = 10$ and $m^* = 0.4m_0$ and in $6H$-SiC, $\kappa = 10$ and $m^* = 0.74m_0$, with m^* defined by $m^* = \sqrt[3]{m_x m_y m_z}$.[26] Thus the electronic wave function has a radius $a^* = 13$ Å for $4H$-SiC and $a^* = 7.2$ Å for $6H$-SiC. The effective-mass ionization
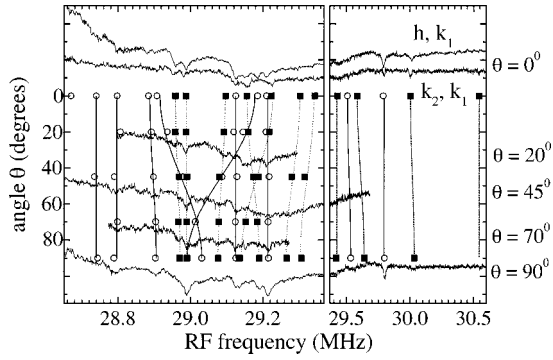
FIG. 8. The orientational dependence of the ^{29}Si ENDOR lines of the three sites h, k_1, and k_2 in $6H$-Si^{13}C. In the upper two spectra, $\angle(\mathbf{B},\mathbf{c})=0°$. The upper spectrum ($\theta=0°$) is measured at position 2, the lower spectrum at position 1. The other four spectra are measured with $\angle(\mathbf{B},\mathbf{c})=20°$, $45°$, $70°$, and $90°$, as indicated on the right. The spectra are measured on the most intense part of the EPR line. Both spectra and points have been corrected for the shift of the nuclear Zeeman frequency when following the EPR line. The open circles and full lines represent the position and dependence of the h-site lines (Table IV) and the filled squares and dotted lines those of the k_1 or k_2 site (Table VI).

TABLE VI. The hf-tensor principal values a and b and the corresponding s and p spin densities of the unpaired electron connected to the k_1 and k_2 site in $6H$-SiC with the ^{29}Si nuclei surrounding the center. Comparison with Table V shows that the tensors are much more anisotropic than the ones connected to the ^{13}C interactions. A distinction between the k_1 and k_2 site tensors is made in the table. The tensors with stars and question marks probably belong to the k_2 site. The unmarked ones belong to the k_1 site. In Fig. 8, all tensors are indicated by dotted lines and full squares.

$6H$-SiC, N, k_1,k_2	^{29}Si, a (MHz)	^{29}Si, b (MHz)	s (%)	p (%)
1*	3.86±0.01		0.084	
2	2.82±0.01	−0.02±0.01	0.061	0.018
3*	2.012±0.003	−0.035±0.002	0.044	0.031
4	1.618±0.008		0.035	
5?	1.402±0.004	0.024±0.003	0.013	0.021
6?	1.322±0.002	0.025±0.002	0.029	0.022
7*	1.107±0.004	0.058±0.003	0.024	0.051
8	1.125±0.002	−0.022±0.002	0.024	0.019
9	0.935±0.001	0.013±0.001	0.020	0.011
10	0.748±0.001		0.016	
11	0.703±0.002	−0.008±0.002	0.015	0.007

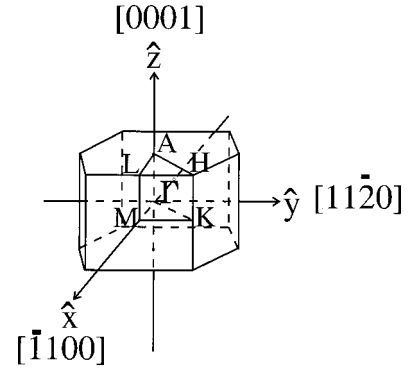FIG. 9. The reciprocal lattice of $4H$-SiC and $6H$-SiC. It is rotated by $60°$ around the c axis with respect to the lattice in real space. The positions of the special symmetry points are shown, together with the orientation of the hexagon with respect to the crystallographic axis system x, y, and z in real space. The Γ point is the center of the hexagon. The M point lies in the $(1\,1\,\bar{2}\,0)$ plane, the K point in the $(\bar{1}\,1\,0\,0)$ plane, and the L point lies above the M point along the $[0\,0\,0\,1]$ direction.

energy E_{eff} of the lowest level is calculated to be $E_{\text{eff}}=54$ meV in $4H$-SiC and $E_{\text{eff}}=101$ meV in $6H$-SiC.

The calculation of the isotropic hf interaction with the ^{13}C and ^{29}Si nuclei

We have calculated the isotropic hf interaction of ^{13}C and ^{29}Si nuclei using the Kohn-Luttinger theory,[5,13,14] in which the interference effect is explicitly taken into account. The isotropic hf interaction is given by

$$A = \tfrac{8}{3}\,\pi_e g_n \beta_e \beta_n \psi(\mathbf{r}_l)|^2, \qquad (1)$$

where g_e is the free-electron g value, g_n is the nuclear g value, β_e is the Bohr magneton, and β_n is the nuclear magneton. $|\psi(\mathbf{r}_l)|^2$ is the donor-electron wave-function density at the lattice site $\mathbf{r}_l$. If we assume that in the ground state the wave function is totally symmetric, i.e., the electron is equally spread over the six minima, then $\psi(\mathbf{r})$ is given by

$$\psi(\mathbf{r}) = \frac{1}{\sqrt{6}} \sum_{j=1}^{6} F_j(\mathbf{r}) u_j(\mathbf{r}) e^{i\mathbf{k}_j \cdot \mathbf{r}_j}. \qquad (2)$$

For the envelope function $F_j(\mathbf{r})$ a variational function is used, which is defined in a local axis system x',y',z', in which the z' axis points from the center of the Brillouin zone Γ towards the jth minimum of the conduction band. The function differs slightly from the one introduced in Ref. 14 or Ref. 5 and is given by

$$F(\mathbf{r}') = \left(\frac{(a^*)^3}{a_{x'} a_{y'} a_{z'}}\right)^{1/2} \exp\left\{-\left(\frac{x'^2}{n^2 a_{x'}^2} + \frac{y'^2}{n^2 a_{y'}^2} + \frac{z'^2}{n^2 a_{z'}^2}\right)^{1/2}\right\}$$
$$\times \exp\left\{-\frac{r'}{na^*}\right\} F_{\text{isa}}(\mathbf{r}'), \qquad (3)$$

where $F_{\text{iso}}(\mathbf{r}')$ is the solution to the isotropic effective mass. The exponents correct F_{ISO} for the anisotropy of the effective
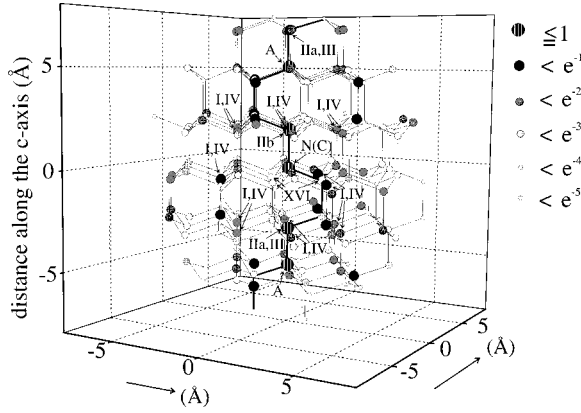
FIG. 10. Results of our calculations for the distribution of the hf interaction around the k site in $4H$-SiC and a tentative assignment of ENDOR lines to nuclei (see discussion). The direction of the c axis is indicated and the values on the axes are in Å. The difference in the value of η for Si, C, or N has not been taken into account and the results were normalized to 1. On the right, the different symbols are explained. The largest, darkest circle is used to indicated all nuclei having a density between 1 and $1/e$, the next largest circle indicates the nuclei with a density between $1/e$ and $1/e^2$, and so on until the smallest, colorless circle that indicates the nuclei with a density smaller than $1/e^5$ of the maximum value.

mass and $n=\sqrt{E_{\mathrm{eff}}/E_{\mathrm{ion}}}$ corrects for the fact that the experimental ionization energy E_{ion} is different from the value E_{eff} calculated on the basis of the effective mass. The square root normalizes the function according to

$$\frac{1}{\Omega}\int_{\mathrm{cell}}|\varphi_j(\mathbf{r})|^2 d\mathbf{r}=1,$$

$$\int |F(\mathbf{r})|^2 d\mathbf{r}=1. \qquad (4)$$

For $F_{\mathrm{iso}}(\mathbf{r}')$ we used $F_{\mathrm{iso}}(\mathbf{r}')=[1/\sqrt{(\pi a^*)^3}]e^{-r'/a^*}$ and the radii $a_{x'}$, $a_{y'}$, and $a_{z'}$ are defined in the same way as a^*. One difficulty in evaluating $|\psi(\mathbf{r}_l)|^2$ at lattice position $\mathbf{r}_l$ is the determination of the value of the amplitude of the Bloch function $u_j(\mathbf{r}_l)$. The value of $u_j(\mathbf{r}_l)$ is independent of j when evaluated at the lattice site $\mathbf{r}_l$, but does depend on the atom (Si or C). An estimate of the square of the wave functions associated with the conduction band at the positions of the nuclei is determined in terms of a dimensionless quantity $\eta \equiv |u_j(\mathbf{r}_l)|^2/\langle u_j(\mathbf{r})\rangle^2_{\mathrm{av}}$, which is used for $u_j(\mathbf{r})^2$ in Eq. (2).[14] As estimated for $u_j(\mathbf{r}_l)^2$, we use $\eta=227$ for $6H$-SiC.[27] In the calculations, the difference in the value of η for Si, C, or N has not been taken into account because the lattice seen from the N center looks the same, whether N substitutes for C or Si, and because the values are not accurately known.

Figure 10 shows the results of our calculations for the distribution of the hf interaction around the k site in $4H$-SiC together with an assignment of ENDOR lines to nuclei discussed below. The results have been normalized to 1. As shown on the right of the figure, the nucleus with the highest density has the darkest color and the largest radius and the nucleus with the smallest density has no color and the small-

est radius. The N nucleus, which has density 1, is indicated by N(C). The largest, darkest circle is used to indicate all nuclei with density between 1 and $1/e$, the next largest circle indicates the nuclei with a density between $1/e$ and $1/e^2$, and so on until the smallest, colorless circle, which indicates the nuclei with a density smaller than $1/e^5$ of the maximum value. The interference effect is clearly visible. It is seen that large spin densities are present on atoms along the c axis above and below the substituted N atom. In contrast, the spin density on the three nearest neighbors of the N atom that are not parallel to the c axis is low. The overall behavior of the spin density is as expected on the grounds of the values of the effective mass and ionization energy. The envelope function of the k site in $4H$-SiC shows a larger Bohr radius than that of the sites in $6H$-SiC because the k site in $4H$-SiC has the smallest effective mass. Since the anisotropy between the masses in $4H$-SiC parallel and perpendicular to **c** is small, the distribution is almost spherical. For the k_1 site in $6H$-SiC, the central hf interaction is slightly smaller. For the h site in $6H$-SiC it is roughly two times smaller than for the k_2 site in $6H$-SiC. Comparing the three centers in $6H$-SiC, it is seen that the distribution of the h site has the largest Bohr radius and the k_2 site the smallest, as expected from the difference in binding energy between the three sites. The main density is distributed on the first-neighbor atom along the c axis and on the three third-neighbor atoms in the plane just below the plane containing the N donor. The large effective mass along the c axis flattens the distribution along this axis.

The assignment of the observed ENDOR lines to specific ^{13}C and [29]Si atoms around the N donor is difficult due to the interference effect. An additional problem is that in $6H$-SiC the position of the minima of the conduction band is not exactly known. Consequently, we are not absolutely sure that the calculated interference effect comes close to the real situation. Moreover, it has been shown by Ivey and Mieher[3,28] in their calculation of the donor wave function in Si that the use of a single conduction band and the use of only the Bloch function at the conduction-band minima may also introduce serious errors. That is why we have mainly used the results of the calculation in a qualitative way to analyze the ENDOR data (in $4H$-SiC) and to explain the differences in the electronic properties of the different N donor sites in $4H$-SiC and $6H$-SiC. The calculations predict a much more shallow (more delocalized) center in $4H$-SiC than in $6H$-SiC, with a corresponding smaller central hf interaction than in $6H$-SiC. In $6H$-SiC, the h site is the most delocalized center and k_2 the most localized one, in agreement with our experimental findings.

Interpretation of the ^{13}C and [29]Si ENDOR data and calculation of the EPR linewidth

We will first discuss the N_k donor in $4H$-SiC because the ENDOR spectra are more informative for this center than for the N donors in $6H$-SiC. The Euler angles of the hf tensors give symmetry information about the shells to which they belong. Moreover, there seems to be a remarkable similarity between the N_k donor in $4H$-SiC on the one hand and the

shallow P (As,Sb) donors in Si on the other hand, when the hf interactions with the impurity nucleus and the surrounding ^{29}Si nuclei are compared. On the basis of this similarity, an assignment of some of the ^{29}Si ENDOR lines to nuclei surrounding the N_k donor is proposed. Tables I and II show, for the N_k donor in 4H-SiC as well as for the P (As) donor in silicon, the hf interactions and spin densities with the impurity atom and the surrounding ^{29}Si nuclei. It is seen that the hf interaction with the central impurity atom leads in both cases to an s-like spin density and that it is of the same order of magnitude. The proposed assignments are indicated in Fig. 10. Looking at Table II, it is seen that line XVI for the N_k donor shows, like the shell with (111) symmetry for the P (As) donor, a remarkably large anisotropic hf interaction, which is almost of the same size as the isotropic one. No other line shows these characteristics. Thus we suggest assigning this line to the three nearest Si neighbors of the N atom in the plane perpendicular to the c axis. This assignment is supported by the calculations that predict a small isotropic hf interaction for these nuclei, and by the Euler angles, which show that the hf tensors point towards these nuclei. Looking at Table II, we see that the lines II and III have a large isotropic hf interaction and axial symmetry along the c axis. Line IIb also has a rather large isotropic hf interaction. The Euler angles as well as a comparison with the (400) shell in Si support an assignment of these lines to nuclei with a large calculated isotropic hf interaction along the c axis, as shown in Fig. 10. We suggest that line IIb, on the grounds of its rather large anisotropic hf interaction, should be assigned to the nearest ^{29}Si neighbor along the c axis, which corresponds to the fourth (111) site in silicon. One more assignment can be suggested. The Euler angles of the lines I and IV are roughly consistent with an assignment to the second Si neighbors of the N atom and the calculations show that there are nuclei in these positions that have a large isotropic hf interaction. A more precise assignment of the lines is considerably more difficult. One of the reasons is that one cannot distinguish between different sites of the same symmetry from symmetry arguments alone and one has to use additional information that is not available for the other lines at the moment. Because most ^{13}C ENDOR lines show no orientational dependence, little symmetry information is known about the hf tensors and thus it is difficult to assign them to nuclei. However, we suggest on the grounds of our calculations that the largest hf interaction, group I in Table III, should be assigned to the nuclei indicated with an A in Fig. 10.

For the N donors in 6H-SiC, a comparison with the donors in Si is not possible because the main density is located on the C atoms in this case. Moreover, the lines are mostly isotropic and thus give no information on the symmetry of the shell or the orientation of the hf tensor. Thus an assignment for these centers should wait for more detailed calculations.

To obtain more information about the N-donor center and the related electronic wave function, we consider the distribution of s and p character. With the table of Morton and Preston,[29] we translate the observed hf interactions into spin density. The isotropic hf interaction (a) gives a measure of

the s spin density (s), whereas the anisotropic hf interaction (b) is a measure for the p density (p). The results are presented in the columns marked by s or p in Tables II and III for the k site in 4H-SiC, in Table IV for the h site in 6H-SiC, and in Tables V and VI for the qc sites in 6H-SiC. Summing up all entries in the s and p column, respectively, it is found that for the k site in 4H-SiC the ratio s:p is 1:4 for the density on the Si atoms and 2.5:1 for the density on the C atoms. For the h, k_1, and k_2 sites in 6H-SiC, we find 1:1 (Si) and 19:1 (C), 3.5:1 (Si) and 6.8:1 (C), and 1.6:1 (Si) and 2:1 (C), respectively. Thus the spin density corresponding to the observed ENDOR lines is p-like in character and located mainly on the Si atoms for the k site in 4H-SiC, whereas for the three sites in 6H-SiC the spin density is s-like in character and located mainly on the C atoms. A small possible error in the ^{29}Si tensor parameters in 6H-SiC does not affect these conclusions and the ensuing conclusions about the band-structure differences.

A possible explanation for the difference in the electronic wave function of the N donor in 4H-SiC and 6H-SiC can be found in the large difference in the band structure of the two polytypes and in the position of the minima in the Brillouin zone. As a result, the linear combination of atomic orbitals describing the wave function of the donor electron is different. Thus the wave function might have a completely different symmetry and a different distribution of s and p character on the Si and C atoms. From band-structure calculations, it is not clear whether Si or C bands lie lowest in the minima in 4H-SiC and 6H-SiC. Our results are consistent with mainly Si-like conduction-band minima in 4H-SiC (bottom of the conduction bands) and C-like conduction-band minima in 6H-SiC.

Our conclusions about the shape and properties of the electronic wave function are based on the interpretation of the observed ENDOR lines. The question arises whether these lines represent the total electron spin density. To calculate this spin density, we must take into account the number of atoms in the shell to which an ENDOR line is assigned. We use 6 for the average number of atoms in a shell, since most lines have not yet been assigned. Though this is an overestimate for the first shells, it is an underestimate for the more distant shells. Using the experimentally observed ENDOR lines and their corresponding spin densities given in Table I–VI, we find for the k site in 4H-SiC $6 \times 3.4\%$ $= 20.4\%$ on the Si atoms and $6 \times 1.1\% = 6.6\%$ on the C atoms. For the h, k_1, and k_2 site in 6H-SiC, we find $6 \times 0.4\% = 2.4\%$ (Si) and $6 \times 1.82\% = 10.92\%$ (C), $6 \times 0.2\%$ $= 1.2\%$ (Si) and $6 \times 1.0\% = 6\%$ (C), and $6 \times 0.3\%$ $= 1.8\%$ (Si) and $6 \times 1.7\% = 10.4\%$ (C), respectively. Thus the spin density found for the k site in 4H-SiC is 27%, whereas for the sites in 6H-SiC the amount of spin density found is less than 14%.

To check whether no important hf interactions have been overlooked, we have calculated the EPR linewidths from the hf interactions of the electron spin with the ^{29}Si and ^{13}C nuclei as determined from the ENDOR measurements. The EPR linewidth at half maximum, ΔB, can be written as[1]

TABLE VII. The calculated [ΔB(Si), ΔB(C)] and measured (ΔB_{exp}) EPR linewidths for the different sites, as well as the total calculated linewidth ΔB_{total} for the nonenriched (natural) as well as the ^{13}C-enriched 4H-SiC and 6H-SiC samples. All values are in mT. The different abundances are indicated in the text. In the enriched 6H-SiC sample, it was not possible to distinguish between the experimental linewidths, ΔB_{exp} (mT), of the three sites. The estimated value of 1 mT is given for all three sites. The estimated error in the other experimental linewidths is 0.05 mT.

Abundance	ΔB(Si) (mT) natural	ΔB(C) (mT)		ΔB_{total} (mT)		ΔB_{exp} (mT)	
		natural	enriched	natural	enriched	natural	enriched
4H-SiC, N_k	0.194	0.084	0.43	0.28	0.62	0.32	0.57
6H-SiC, N_h	0.063	0.176	0.99	0.26	1.05	0.30	~1
6H-SiC, N_{k1}	0.066	0.102	0.58	0.17	0.64	0.25	~1
6H-SiC, N_{k2}	0.092	0.165	0.88	0.25	0.97	0.30	~1

$$\Delta B^2 = 2\left[\sum_i^R f(\text{Si})n_i(\text{Si})\left(\frac{a_i(\text{Si})}{2}\right)^2 + \sum_j^M f(\text{C})n_j(\text{C})\left(\frac{a_j(\text{C})}{2}\right)^2\right],$$

where n_i and n_j are the number of equivalent sites in the ith Si shell and the jth C shell. a_i and a_j are the hf interactions for equivalent sites in the ith Si shell and in the jth C shell. f(Si) and f(C) are the fractional abundances of [29]Si and [13]C [f(Si)=0.047 and f(C)=0.011 in natural abundance samples, in enriched 4H-SiC f(C)=0.3, and in enriched 6H-SiC f(C)=0.35]. f(Si)n_i(Si) and f(C)n_j(C) are the probabilities of having the ith and jth lattice sites occupied with a [29]Si or ^{13}C, respectively. The summations extend over the R silicon shells and the M carbon shells, which contribute to the EPR linewidth. In our calculation, we include only those shells that have an isotropic hf interaction that is larger than 1 MHz. We use 6 for the amount of nuclei in a shell. In the case of the isotopically enriched ^{13}C sample, the number of ^{13}C nuclei with which the donor electron interacts is greatly enhanced and thus the linewidth increases. The results of the calculation as well as the experimental values, ΔB_{exp}, are shown in Table VII. The linewidth due to the C atoms, ΔB(C), and the total linewidth, ΔB_{total}, is given for the nonenriched (natural) as well as for the enriched case. From Table VII, it is clear that the calculations agree very well with the experimentally found linewidth. From this it can be concluded that we did not miss large hf interactions with neighboring [29]Si or ^{13}C atoms.

A large part of the spin density is related to the nonresolved ENDOR signal around the Si and C nuclear Zeeman frequencies, which consists of a superposition of a large number of ENDOR lines with a very small hf interaction. In delocalized centers, this signal is expected to be very pronounced; in localized centers it is almost not present. Inspection of the spectra in Fig. 2 shows that the nonresolved signal is indeed very pronounced, with an estimated width of 1.1

MHz. In contrast, for the B-acceptor center[4] about 100% spin density is found back in the resolved ENDOR hf lines and no nonresolved signal is present. The amount of spin density incorporated in the nonresolved signal can be estimated using the approximation that the hf interaction $A(r)$ is given by $A(r)=A_0 \exp(-r/r_B)$, with A_0 the spin density at the center and r_B the Bohr radius of the wave function. The amount of spin density in a shell δr at distance r from the center is given by the product of the spin density ρ at r, calculated from $A(r)$, and the number of atoms in δr. $\rho(r)$ has a maximum at twice the Bohr radius. Using, for example, $r_B = 7.2$ Å and $A_0 = 4$ MHz, 60% of the spin density turns out to originate from nuclei located between 9 and 30 Å [$A(9$ Å$)<1.1$ MHz]. Increasing r_B even further, it is possible to account for an even larger amount of spin density. Thus it seems reasonable to assume that the main part of the spin density is located in the crystal at distances of twice the Bohr radius and beyond.

The hf interaction with the ^{14}N nucleus

It is interesting to compare the spin density on the ^{14}N nucleus with that on the surrounding ^{13}C and [29]Si nuclei. Assuming that the wave function of the N donor corresponds to the totally symmetric combination of the wave functions of the six minima of the conduction band,[25] we expect that this spin density is maximal on the central ^{14}N nucleus. This is indeed the case for these sites in 4H-SiC and 6H-SiC. From Tables I–III it is seen that the spin density on the ^{14}N nucleus of the qc sites is about 2%. On the [29]Si nuclei in 4H-SiC, the highest spin density is 1.3% (on the ^{13}C nuclei it is even lower) and on the ^{13}C nuclei in 6H-SiC it is 0.3% (on the [29]Si nuclei it is even lower). In contrast, for the h site in 6H-SiC the spin density on the ^{14}N nucleus amounts to about 0.3%, which is the same as the maximum spin density on the [29]Si nuclei.

A possible explanation for this difference in behavior for the qc and h sites may be found in the interference effect, assuming that the center of the donor electronic wave func-

tion is on the N atom in the case of the qc sites but slightly displaced in the case of the h site. If true, the interference effect would then lead to a maximum value for the spin density on the ^{14}N nucleus in the qc sites but to a reduced value in the case of the h site.

The substitutional position of the N atom

The question is whether our ENDOR results might give an indication about the substitutional position of the N atom in the $4H$-SiC and $6H$-SiC lattices. Interestingly, the band-structure calculations of Fukumoto[30] predict that the main spin density should be on the Si atoms in the case of a N_C substitution and on the C atoms in the case of a N_{Si} substitution. Following these ideas, we might conclude that N resides on a C position in $4H$-SiC and on a Si position in $6H$-SiC. The same calculations predict N_C to be a shallow center and N_{Si} to be a deep center. However, from Table I it is clear that there is no connection between the observed hf interactions and the ionization energies of the different sites in $4H$-SiC and $6H$-SiC. We note further that in $6H$-SiC the spatial distribution of the spin density over ^{13}C and ^{29}Si atoms is qualitatively the same for the h, k_1, and k_2 sites, although the hf interaction of ^{14}N in h and qc sites differs considerably. Thus at the present stage we have no compelling argument to change the current point of view that N substitutes for a C atom in the SiC lattice.

V. CONCLUSION

The distribution of the electronic wave function of the N donor function in the k site in $4H$-SiC and in the h, k_1, and k_2 sites in $6H$-SiC has been determined from the isotropic and anisotropic hf interaction of the unpaired electron spin with the ^{13}C and ^{29}Si nuclei. It appears that the spin-density distribution over the ^{13}C and ^{29}Si nuclei differs between the $4H$-SiC and $6H$-SiC polytypes. The same conclusion is drawn from the EPR line broadening of the N donor in ^{13}C-enriched $4H$-SiC and $6H$-SiC. The main part of the spin density in $4H$-SiC is located on the Si sublattice and the wave function contains a relatively large portion of Si p character. For the three sites in $6H$-SiC, the main part of the spin density is located on the C sublattice and the wave function is built mostly of s-like C atomic orbitals. Comparing the three sites in $6H$-SiC, the h-site wave function has the largest delocalization and is most isotropic. In the k_2 site, the wave function is most localized and least isotropic. The larger part of the spin density is located far into the crystal. The difference in the behavior of the wave function in the $4H$ and $6H$ polytypes seems to be due to the difference in their conduction-band structure. Our results are consistent with mainly Si-like conduction-band minima in $4H$-SiC (bottom of the conduction bands) and C-like conduction-band minima in $6H$-SiC.

[1] G. Feher, Phys. Rev. **114**, 1219 (1959).

[2] R. C. Fletcher, W. A. Yager, G. L. Pearson, A. N. Holden, W. T. Read, and F. R. Merritt, Phys. Rev. **94**, 1392 (1954); R. C. Fletcher, W. A. Yager, G. L. Pearson, and F. R. Merritt, *ibid.* **95**, 844 (1954).

[3] J. L. Ivey and R. L. Mieher, Phys. Rev. B **11**, 849 (1975), and earlier papers referenced therein.

[4] A. v. Duijn-Arnold, J. Mol, R. Verberk, J. Schmidt, E. N. Mokhov, and P. G. Baranov, Phys. Rev. B **60**, 15 829 (1999).

[5] W. J. Choyke and L. Patrick, Phys. Rev. **127**, 1868 (1962); W. J. Choyke, D. R. Hamilton, and L. Patrick, *ibid.* **133**, 1163 (1964).

[6] P. J. Colwell and M. V. Klein, Phys. Rev. B **6**, 498 (1972).

[7] H. H. Woodbury and G. W. Ludwig, Phys. Rev. **124**, 1083 (1961); G. W. Ludwig and H. H. Woodbury, Solid State Phys. **13**, 223 (1962).

[8] G. E. G. Hardeman and G. B. Gerritsen, Phys. Rev. Lett. **20**, 623 (1966).

[9] L. Patrick, Phys. Rev. B **5**, 2198 (1972); L. Patrick, Phys. Rev. **138**, 1477 (1965).

[10] E. N. Kalabukhova, N. N. Kabdin, and S. N. Lukin, Fiz. Tverd. Tela (Leningrad) **29**, 2532 (1987) [Sov. Phys. Solid State **29**, 1461 (1987)].

[11] S. Greulich-Weber, M. Feege, J.-M. Spaeth, E. N. Kalabukhova, S. N. Lukin, and E. N. Mokhov, Solid State Commun. **93**, 393 (1995).

[12] S. Greulich-Weber, Phys. Status Solidi A **162**, 95 (1997), and references therein.

[13] W. Kohn and J. M. Luttinger, Phys. Rev. **97**, 1721 (1955).

[14] W. Kohn, in *Solid State Physics*, edited by F. Seitz and D. Turnbull (Academic, New York, 1957), Vol. 5, pp. 257–320.

[15] Yu. A. Vodakov, E. N. Mokhov, M. G. Ramm, and A. D. Roenkov, Krist. Tech. **5**, 729 (1979).

[16] E. I. Radovanova, R. G. Verenchikova, and Yu. A. Vodakov, Fiz. Tekh. Poluprovodn. **17**, 1115 (1983) [Sov. Phys. Semicond. **17**, 640 (1983)].

[17] T. Matsumoto, O. G. Poluektov, P. G. Baranov, E. N. Mokhov, and J. Schmidt, Phys. Rev. B **55**, 2219 (1997).

[18] R. T. Weber, J. A. J. M. Disselhorst, L. J. Prevo, J. Schmidt, and W. Th. Wenckebach, J. Magn. Reson. **81**, 129 (1989); J. A. J. M. Disselhorst, H. van der Meer, O. G. Poluektov, and J. Schmidt, *ibid.* **115**, 183 (1995).

[19] W. B. Mims, in *Electron Paramagnetic Resonance*, edited by S. Geschwind (Plenum, New York, 1972).

[20] N. M. Atherton, *Principles of Electron Spin Resonance* (Ellis Horwood Ltd., Chichester, 1993).

[21] V. G. Grachev, Zh. Eksp. Teor. Fiz. **92**, 1834 (1987) [Sov. Phys. JETP **65**, 7029 (1987)].

22 An-Ban Chen and P. Srichaikul, Phys. Status Solidi B **202**, 81 (1997).

23 N. T. Son, O. Kordina, A. O. Konstantinov, W. M. Chen, E. Sorman, B. Monemar, and E. Janzen, Appl. Phys. Lett. **65**, 3209 (1994); N. T. Son, W. M. Chen, O. Kordina, A. O. Konstantinov, B. Monemar, E. Janzen, D. M. Hofmann, D. Volm, M. Drechsler, and B. K. Meyer, *ibid.* **66**, 1074 (1995); W. M. Chen, N. T. Son, E. Janzen, D. M. Hofmann, and B. K. Meyer, Phys. Status Solidi A **162**, 79 (1997).

24 R. P. Devaty and W. J. Choyke, Phys. Status Solidi A **162**, 5 (1997).

25 *Silicon Carbide, A Review of Fundamental Questions and Applications to Current Device Technology*, edited by W. J. Choyke, H. Matsunami, and G. Pensl (Akademie Verlag, Berlin, 1997) [special edition of Phys. Status Solidi B **202** (1997)].

26 W. L. R. Lambrecht, S. Limpijumnong, S. N. Rashkeev, and B. Segall, Phys. Status Solidi B **202**, 5 (1997).

27 M. N. Alexander, Phys. Rev. **172**, 331 (1968).

28 J. L. Ivey and R. L. Mieher, Phys. Rev. B **11**, 822 (1972).

29 J. R. Morton and K. F. Preston, J. Magn. Reson. **30**, 377 (1978).

30 A. Fukumoto, Phys. Status Solidi B **202**, 125 (1997).